*HIGH ENERGY PHENOMENA IN MASSIVE STARS*
*ASP Conference Series, Vol. 422, © 2010*
*J. Martí, P. L. Luque-Escamilla, and J. A. Combi, eds*

# Gamma-Rays from Massive Protostars

Gustavo E. Romero and Anabella T. Araudo

*Instituto Argentino de Radioastronomía (CCT La Plata, CONICET), C.C.5, 1894 Villa Elisa, Buenos Aires, Argentina*
*Facultad de Ciencias Astronómicas y Geofísicas, Universidad Nacional de La Plata, Paseo del Bosque, 1900 La Plata, Argentina*

Valentí Bosch-Ramon

*Max Planck Institut für Kernphysik, Saupfercheckweg 1, Heidelberg 69117, Germany*

Josep M. Paredes

*Departament d'Astronomia i Meteorologia and Institut de Ciències del Cosmos (ICC), Universitat de Barcelona (UB/IEEC), Martí i Franquès 1, 08028, Barcelona, Spain*

**Abstract.** Massive protostars have associated bipolar outflows with velocities of hundreds of km $s^{-1}$. Such outflows produce strong shocks when interact with the ambient medium leading to regions of non-thermal radio emission. Under certain conditions, the population of relativistic particles accelerated at the terminal shocks of the protostellar jets can produce significant gamma-ray emission. We estimate the conditions necessary for high-energy emission in the non-thermal hot spots of jets associated with massive protostars embedded in dense molecular clouds. Our results show that particle-matter interactions can lead to the detection of molecular clouds hosting massive young stellar objects by the *Fermi* satellite at MeV-GeV energies and even by Cherenkov telescope arrays in the GeV-TeV range. Astronomy at gamma-rays can be used to probe the physical conditions in star forming regions and particle acceleration processes in the complex environment of massive molecular clouds.

## 1. Introduction

Massive stars appear to be formed in the dense cores of massive cold clouds (see Garay & Lizano 1999, and references therein). The accumulation of gas in the core might proceed through previous stages of fragmentation and coalescence progressively generating a massive protostar that then accretes from the environment (e.g. Bonnell, Bate, & Zinnecker 1998). An alternative picture is direct accretion onto a central object of very high mass (e.g. Rodríguez et al. 2008) (see Shu, Adams, & Lizano 1987, for the basic mechanism). In any case, the prestellar core is expected to have angular momentum which would lead to the formation of an accretion disk. The strong magnetic fields inside the cloud that thread the disk should be pulled toward the protostar and twisted by the

rotation giving rise to a magnetic tower, with the consequent outflows, as shown by numerical simulations (e.g. Banerjee & Pudritz 2007).

Evidence supporting the existence of molecular outflows is found through methanol masers, which are likely associated with shocks formed by the interaction with the external medium (e.g. Plambeck & Menten 1990). However, the most important piece of evidence for outflows is in the form of thermal radio jets. These jets are observed to propagate through the cloud material along distances of a fraction of a parsec in some cases (e.g. Martí, Rodríguez, & Reipurth 1993). At the end point of the jets, hot spots due to the terminal shocks are observed in several sources. In a few cases, these hot spots are clearly non-thermal, indicating the presence of relativistic electrons that produce synchrotron radiation (e.g. Araudo et al. 2007, 2008).

A population of relativistic particles in the complex environment of the massive molecular cloud where the protostar is being formed will produce high-energy radiation through a variety of processes: inverse Compton (IC) up-scattering of IR photons from the cloud, relativistic Bremsstrahlung, and, if protons are accelerated at the shock as well, inelastic proton-proton (*pp*) collisions. If such a radiation is detectable, $\gamma$-ray astronomy can be used to shed light on the star forming process, the protostar environment, and cosmic ray acceleration inside molecular clouds. In the present contribution we want to discuss the conditions under what massive protostars can produce $\gamma$ rays detectable by the *Fermi* satellite in the immediate future, and also whether Cherenkov telescopes may eventually detect these sources. The models presented here incorporate many refinements from the simpler approach published by Araudo et al. (2007).

## 2. Basic Scenario

The basic scenario has been outlined in Fig.1 of Araudo et al. (2007). A massive young stellar object (YSO), or a group of them, is embedded into a molecular cloud. The protostar heats the cloud in such a way that it can be detected as a strong IR source, with luminosities in the range $L_{\rm IR} \sim 10^{4-5}\ L_\odot \sim 10^{38-39}$ erg s$^{-1}$ whereas the optical counterpart is obscured by the cloud. Masses and sizes of these clouds are of the order of $\sim 10^3\ M_\odot$ and few pc, respectively (see Garay & Lizano 1999). The thermal jets can propagate up to distances of $10^{16-18}$ cm from the central source, and the non-thermal radio lobes are seen at distances of $\sim$ pc from the protostar (Martí, Rodríguez, & Reipurth 1993; Garay et al. 2003) with sizes of the order of 1 % this distance. The radio lobes are ionised by the terminal shocks and particles can be accelerated up to relativistic energies both in the reverse shock, as well as in the forward shock in the ionised gas. In what follows we will discuss the characteristics of the non-thermal particle population of the lobes arose from forward and reverse shocks.

A crucial parameter for the acceleration of particles up to high energies is the magnetic field $B$. Equipartition calculations with the non-thermal population of particles (Araudo et al. 2007) and Zeeman measurements (e.g. Crutcher 1999) suggest $B \sim 1$ mG. Magnetic fields are thought to play an important role supporting the cloud before the gravitational collapse, allowing high densities in the cores to be achieved (e.g. McKee & Ostriker 2007). The medium density

strongly determines the jet evolution, and is a key factor regarding the emission at high energies.

Here, we consider the effect of both a forward and a reverse shock, the escape of the particles from the acceleration region, and the illumination of the whole molecular cloud by protons that diffuse from the lobes, among others refinements with respect to our previous work. The cloud acts as reservoir of locally accelerated cosmic rays. In very massive clouds, where several protostars are forming, this effect can be very significative.

## 3. Particle Acceleration and Losses

The diffusive shock acceleration process (DSA, e.g. Drury 1983) can operate in the turbulent region at the termination of the thermal jets. If the jet head is still moving in the free propagation phase, the bow shock in the cloud can be as fast as the jet, but then the shock luminosity must be smaller than the one carried by the jet ($L_{\rm j}$). In any case, regardless the energy budget, the fast velocities allow particle acceleration up to very high energies.

On the other hand, when the swept cloud material is massive enough, the jet slows down and the bow shock produced by the interaction can be as slow as $\sim 10$ km s$^{-1}$. The shocked material of the cloud will be radiative, forming a very thin shell pushed by the jet. This shock is not suitable to accelerate particles, but its downstream material would be a good target for *pp* interactions or relativistic Bremsstrahlung in case that electrons and protons accelerated elsewhere could reach it. In the slow bow shock case, the region suitable for particle acceleration is the reverse shock formed in the jet, which was not strong when the bow shock was moving as fast as the jet itself (being an effective accelerator). When the bow shock has slowed significantly down, the reverse shock has a velocity $v_{\rm s} \sim v_{\rm jet}$. The shock luminosity in the slow bow shock case is similar to the jet one.

In any case (bow shock or reverse shock acceleration), the particle acceleration rate for a parallel non-relativistic strong shock in the test particle approximation is

$$\left.\frac{dE_{e,p}}{dt}\right|_{\rm gain} \sim \eta q B c, \qquad \eta = \frac{3}{20 f_{\rm sc}} \left(\frac{v_{\rm s}}{c}\right)^2, \tag{1}$$

where $e$ and $p$ stand for electrons and protons, respectively (e.g. Protheroe 1999). The parameter $f_{\rm sc}$ is the ratio of the mean free path of the particles to their gyro-radius $r_{\rm g}$. Close to the Bohm limit, where the diffusion coefficient is $D_{\rm B} = c r_{\rm g}/3$, $f_{\rm sc} \sim 1$. For outflows with bulk velocities $v_{\rm jet} \sim 10^3$ km s$^{-1}$ (e.g. Martí, Rodríguez, & Reipurth 1995) we get a relatively low efficiency of $\eta \sim 10^{-6}$, which is, nonetheless, enough to achieve relativistic energies for the particles.

### 3.1. Hadronic Losses

The relevant energy loss for protons is due to *pp* collisions with the nuclei of the ambient gas of density $n$:

$$\left.\frac{dE_p}{dt}\right|_{pp} = n\, c\, \sigma_{pp}(E_p) K_{pp} E_p, \tag{2}$$

where $\sigma_{pp}(E_p) = 34.3 + 1.88L + 0.25L^2$ mb, with $L = \ln(E_p/1\ \mathrm{TeV})$, is the interaction cross section (Kelner, Aharonian, & Vugayov 2006) and $K_{pp} \sim 0.5$ the inelasticity. The emission from *pp* interactions can be significant from high- to very high-energy $\gamma$ rays.

In addition to the radiative losses, protons can escape from the emitting region of size $l_{\rm lobe}$ by diffusion or convection downstream the shock, in accordance with the timescales of these processes: $t_{\rm diff} \sim l_{\rm lobe}^2/2\,D_{\rm B}$ and $t_{\rm conv} \sim 4\,l_{\rm lobe}/v_{\rm s}$. The escape time $t_{\rm esc}$ is defined as the minimum between $t_{\rm diff}$ and $t_{\rm conv}$. In the presence of a turbulent $B \sim 1$ mG or higher, $t_{\rm conv}$ will usually be shorter than $t_{\rm diff}$ and $t_{pp} = E_p(dE_p/dt)_{pp}^{-1}$. Nevertheless, in the cases studied here the most energetic protons have their energy constrained by diffusive escape upstream.

### 3.2. Leptonic Losses

The main losses for electrons are due to synchrotron radiation, IC up-scattering of IR photons, and relativistic Bremsstrahlung. The standard formulae are presented, for instance, in Blumenthal & Gould (1970). Synchrotron and IC losses in the Thomson regime satisfy:

$$\left(\left.\frac{dE_e}{dt}\right|_{\rm synch}\right)\left(\left.\frac{dE_e}{dt}\right|_{\rm IC}\right)^{-1} = \frac{u_B}{u_{\rm ph}} > 1, \qquad (3)$$

where $u_B = B^2/8\pi$ is the magnetic energy density ($\sim 10^{-8}$ erg cm$^{-3}$ for $B = 1$ mG), and $u_{\rm ph}$ is the photon energy density inside the cloud, typically $u_{\rm ph} \sim 10^{-9}$ erg cm$^{-3}$, which is dominated by IR photons. This means that synchrotron losses will dominate over IC cooling. The highest energy electrons will cool via synchrotron and they will radiate from radio to soft X-rays through this mechanism. On the other hand, lower energy electrons are dominated by relativistic Bremsstrahlung and escape losses from the emitter. The relativistic Bremsstrahlung component contributes to the spectrum from hard X-rays up to high energies.

For very high densities, ionization/Coulomb collision losses may dominate radio emitting electrons, hardening their spectra. An observed steep radio spectrum implies that this cooling channel is minor in comparison to synchrotron radiation.

### 3.3. Maximum Energies and Particle Spectra

In the Bohm limit we expect for electrons that the maximum energy will be determined by the radiative losses. Equating energy gains and losses we get, for the parameters of the basic scenario sketched in Sect.2., that $E_e^{\rm max} \sim 1$ TeV. For protons, on the contrary, cooling times are longer and hence they can diffuse away from the shock upstream into the cloud. The residence time in the shock region, of size $\sim l_{\rm lobe}$, determines the maximum energy: $E_p^{\rm max} \sim 1 - 100$ TeV.

The particle distributions $N_{e,p}(t, E_{e,p})$ are given by the transport equation (e.g. Ginzburg & Syrovatskii 1964):

$$\frac{\partial N_{e,p}\,(t, E_{e,p})}{\partial t} + \frac{\partial\left[b_{e,p}(E_{e,p})N_{e,p}\,(t, E_{e,p})\right]}{\partial E_{e,p}} + \frac{N_{e,p}\,(t, E_{e,p})}{t_{\rm esc}} = Q_{e,p}(t, E_{e,p}), \quad (4)$$

where $Q_{e,p}(t, E_{e,p}) \propto E_{e,p}^{-\Gamma_{e,p}}$ is the function for the particle injection (a power law according to the DSA mechanism which is supposed to operate in the radio lobes). Injection takes place during the lifetime of the source ($t_{\rm life}$), estimated typically in $t_{\rm life} \sim 100 - 1000$ yr $\approx 3 \times (10^9 - 10^{10})$ s for massive O protostars (see Garay et al. 2003). In the transport equation $t$ is time, and $b_{e,p}(E_{e,p})$ is the summation of all energy losses.

Eq. (4) can be solved in the steady state setting $\partial N_{e,p}\left(t, E_{e,p}\right)/\partial t = 0$. In the cases when synchrotron dominates over escape or relativistic Bremsstrahlung, the electron distribution will be $N_e(E_e) \propto Q_e E_e^{-1}$ at high energies. Relativistic Bremsstrahlung losses and escape, on the contrary, lead to $N_e(E_e) \propto Q_e(E_e)$. The injected proton spectrum is not modified since the relevant losses, due to inelastic *pp* collisions, are almost linear with the energy in the range considered (from $\sim$ 100 MeV to TeV) $N_p(E_p) \propto Q_p$.

The normalization of the electron spectrum is given by the observed radio luminosities, between $10^{28}$ and $10^{30}$ erg s$^{-1}$ for sources like HH 80/HH 81 (Martí, Rodríguez, & Reipurth 1993) and IRAS 16547−4247 (Rodríguez et al. 2005). The proton to electron energy density ratio, $a = u_p/u_e$, cannot be established from first principles in the acceleration process and it should be considered as a phenomenological parameter. All this fixes the luminosity injected in non-thermal particles ($L_{\rm nt}$). In the next section we will consider two cases: one with only electrons ($a = 0$) and another dominated by protons, with a ratio $a = 100$, as observed in galactic cosmic rays.

## 4. Non-thermal Spectral Energy Distributions

Once the particle energy distribution $N_{e,p}(E_{e,p})$ has been obtained through Eq. (4), the spectral energy distribution (SED) can be calculated as:

$$E_\gamma L_{E_\gamma} = E_\gamma^2 \int q_\gamma(E_\gamma, E_{e,p}) N_{e,p}(E_{e,p}) dE_{e,p}, \tag{5}$$

where $q_\gamma$ is the particle emissivity of the particular radiation process and $L_{E_\gamma}$ is the specific luminosity.

### 4.1. IRAS 16547−4247

The powerful IR source IRAS 16547−4247 is composed by a massive protostar embedded in a very dense and luminous molecular cloud (Garay et al. 2003). In addition, two radio lobes are at the end of the thermal jets of the central YSO, being the south one clearly non-thermal.

In Fig.1 we show an example of the SED for the non-thermal lobe of the IRAS source, where only primary electrons have been considered. In this specific case, the reverse shock is accelerating particles since the cloud material is very dense and the bow shock has been already slowed down. Densities have been taken as high as possible accounting for the ionization cooling limit. The parameters used in the modeling are presented in Table 1. This example shows that, despite the IC contribution is negligible, $\gamma$-rays might still be of leptonic origin if densities are particularly high. The spectral shape is determined by the escape of electrons from the emitter (this was not considered in Araudo et al. 2007). The SED has two clear peaks, one due to synchrotron radiation

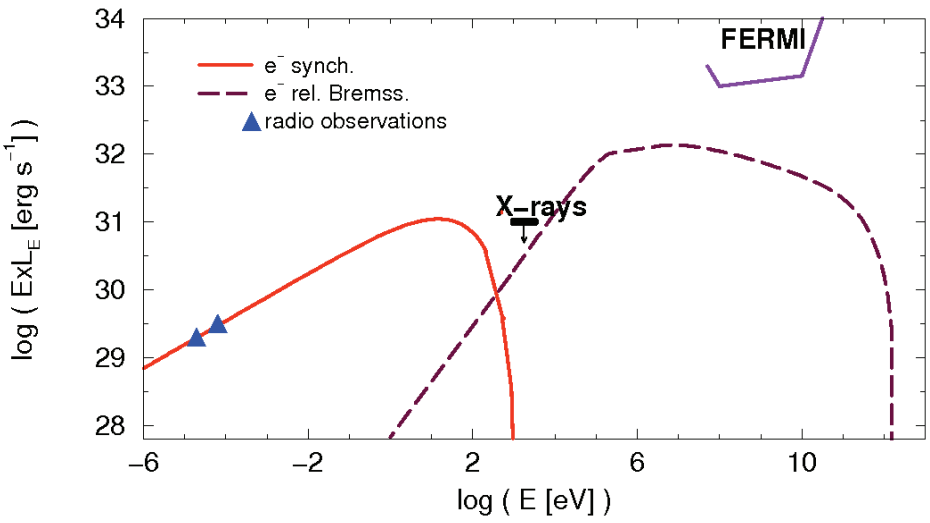


Figure 1. SED of the south lobe of the source IRAS 16547−4247 for a pure leptonic case (a=0). The IC contribution is negligible and not shown here. Radio and X-ray observational points are from Rodríguez et al. (2005) and from Araudo et al. (2007), respectively.

and the second one due to relativistic Bremsstrahlung. The latter emission extends into the $\gamma$-ray domain with integrated luminosities of $\sim 5 \times 10^{32}$ and $3 \times 10^{31}$ erg s$^{-1}$ at $E_\gamma \sim 0.1 - 100$ and $> 100$ GeV, respectively. The emission for the case with $a = 100$ has been also estimated but not shown in the present paper. Synchrotron emission is now dominated by secondary pairs, and the *pp* in the lobe reaches integrated luminosities of $\sim 2 \times 10^{33}$ and $2 \times 10^{32}$ erg s$^{-1}$ at $E_\gamma \sim 0.1 - 100$ and $> 100$ GeV, respectively.

### 4.2. HH 80-81 System

The Herbig-Haro objects HH 80 and HH 81 are located at the terminal point of a massive YSO jet. The triple system composed by the central YSO plus HH 80, HH 81 and HH 80 North is at the edge of a dark cloud (Martí, Rodríguez, & Reipurth 1993).

In Fig.2, we show a case dominated by protons, with $a = 100$, for the source HH 80. Given the lower densities of the environment, the bow shock could still move fast and therefore be an efficient particle accelerator. In this source the radio emission is still produced by primary electrons, with some contribution from secondary pairs injected through the decay of charged pions. At high energies the IC and the relativistic Bremsstrahlung are negligible and the emission is dominated by $\gamma$ rays originated in neutral pion decays from *pp* interactions. The $\gamma$-ray cutoff appears at energies $E_\gamma^{\rm max} \sim E_p^{\rm max}/10$. The total $\gamma$-ray integrated luminosities from the lobe can reach $\sim 10^{32}$ erg s$^{-1}$. However, since protons can diffuse out the acceleration region with significant energy due to their long cooling times, the interaction with the cold material of the cloud will add a diffuse component (Aharonian & Atoyan 1996). This emission could look

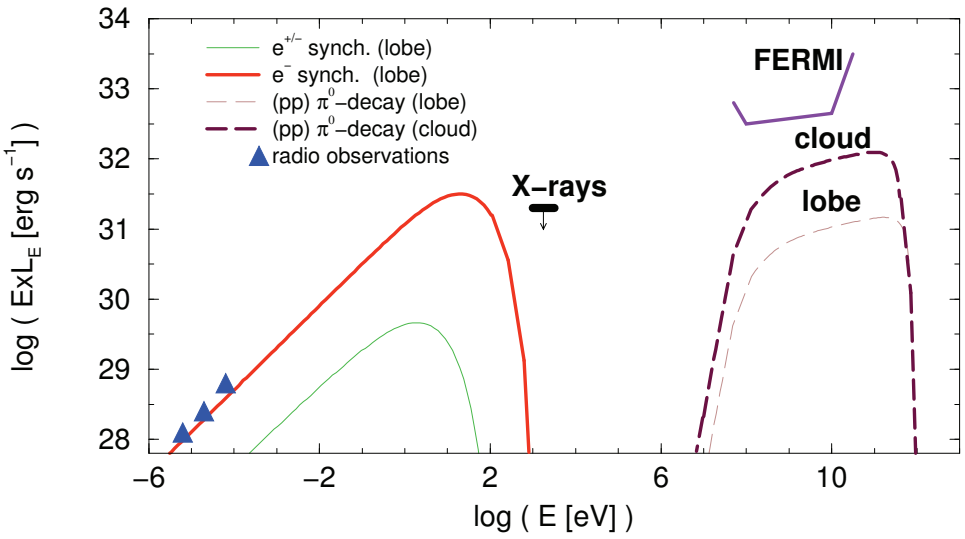


Figure 2. SED of the source HH 80 for a case dominated by protons ($a = 100$). The synchrotron radiation is dominated by primary electrons. Radio and X-ray observational points are from Martí, Rodríguez, & Reipurth (1993) and Pravdo, Tsuboi, & Maeda (2004), respectively. Both the emission from the lobe and that which results from the proton diffusion in the cloud are shown. In both figures we indicate the sensitivity curve of *Fermi* for 1 yr of observations and the distance of the sources, $\sim 3$ and 1.7 kpc for IRAS 16547−4247 and HH 80-81, respectively.

marginally extended for current Cherenkov telescopes and *Fermi*. The diffuse radiation from the massive molecular cloud can increase the $\gamma$-ray integrated luminosity to the level of $\sim 5 \times 10^{32}$ and $6 \times 10^{32}$ erg s$^{-1}$ at $E_\gamma \sim 0.1 - 100$ and $> 100$ GeV, respectively, rendering the source detectable. The leptonic case (a=0) for the object HH 80 was also computed but the luminosities at high energies are well below $10^{30}$ erg s$^{-1}$ and the spectra are not shown here.

## 5. Summary and Discussion

In the present contribution, we study the production of $\gamma$-ray emission at the terminal points of jets that emanate from massive protostars. In particular, we consider two sources: IRAS 16547−4247 and HH 80/HH 81. In the former case, ralativistic particles are accelerated in the shocked jet, wereas in the latter, in the bow shock. With the model presented here, $\gamma$-ray luminosities up to $\sim 10^{32}$ erg s$^{-1}$ are obtained.

As pointed out by Romero (2008), the detection of massive protostars at $\gamma$-ray energies would open a new window to star formation studies. The detection of the cutoff in the SED will give important insights on the acceleration efficiency in the terminal shocks of the outflows. This, in turn, can be used to constrain the shock velocity and the diffusion coefficient. The accumulation of cosmic rays accelerated in the radio lobes into the molecular cloud can produce extended $\gamma$-ray sources.

Table 1. Physical parameters considered in this work.

| | IRAS 16547−4247 | HH 80 | Cloud |
|---|---|---|---|
| $l_{\rm lobe}$ [cm] | $1.1 \times 10^{16}$ | $5 \times 10^{16}$ | |
| $L_{\rm j}$ [erg s$^{-1}$] | $10^{36}$ | $1.5 \times 10^{36}$ | |
| $t_{\rm dyn}$ [a] [s] | $4 \times 10^{8}$ | $3 \times 10^{9}$ | $10^{11}$ |
| $a$ | 0 | 100 | |
| $n$ [cm$^{-3}$] | $10^{6}$ | $10^{3}$ | $2.5 \times 10^{2}$ |
| $B$ [mG] | 1 | 0.3 | |
| particle | $e$ | $p$ | |
| $L_{\rm nt}/L_{\rm j}$ | 0.02 | 0.1 | |
| $\Gamma$ | 2.2 | 1.8 | |

[a] Dominant timescale: it is approximately $t_{\rm life}$ for HH 80 and the cloud, and $t_{\rm esc}$ for the IRAS source.

The combined effect of several protostars deeply embedded in giant clouds might be responsible for GeV-TeV sources found in star forming regions by EGRET, *Fermi*, *AGILE* and Cherenkov telescopes. A clustering of gamma-ray sources should be present in regions with large molecular clouds and star formation, as already inferred from EGRET data (e.g. Romero, Benaglia, & Torres 1999). Although we do not expect that massive protostars should be among the bright sources detected by *Fermi* (Abdo et al. 2009), our predictions show that they should show up in further analysis of weaker sources after few years of observations. The emission levels above 100 GeV, of about 0.01 Crab, could be detectable by current and future Cherenkov telescopes for $\sim 50$ hours observation time.

Cosmic-ray re-acceleration inside the clouds due to magnetic turbulence (e.g. Dogiel et al. 2005) could result in stronger sources. Neither UV nor hard X-ray counterparts related to thermal Bremsstrahlung produced in the shock downstream regions are expected to be observed from these sources because of the large absorption and/or low emission levels. In any case, massive clouds with high IR luminosities and maser emission (tracers of massive star formation) deserve detailed study with *Fermi* and other $\gamma$-ray telescopes.

**Acknowledgments.** G.E.R. and A.T.A. are supported by the Argentine agency ANPCyT. G.E.R., V.B-R., and J.M.P acknowledge support by the Ministerio de Educación y Ciencia (Spain) under grant AYA 2007-68034-C03-01, FEDER funds. A.T.A. thanks Max Planck Institut fuer Kernphysik for his kind hospitality and suport. V.B-R. gratefully acknowledges support from the Alexander von Humboldt Foundation. The authors thank very much Josep Martí for organizing an excelent and enjoyable workshop.

**References**

Abdo, A.A., et al. 2009, arXiv0902.1340
Aharonian, F.A., & Atoyan, A.M. 1996, A&A, 309, 917
Araudo, A.T., et al. 2007, A&A, 476, 1289
Araudo, A.T., et al. 2008, IJMP D, 17, 1889

Banerjee, R., & Pudritz, R.E. 2007, ApJ, 660, 479
Blumenthal, G.R., & Gould, R.J. 1970, Rev. Mod. Phys., 42, 237
Bonnell, I.A., Bate, M.R., & Zinnecker, H. 1998, MNRAS, 298, 93
Crutcher, R.M. 1999, ApJ, 520, 706
Dogiel, V.A., et al. 2005, Ap&SS, 297, 201
Drury, L.O'C. 1983, Reports on Progress in Physics, 46, 973
Garay, G., & Lizano, S. 1999, PASP, 111, 1049
Garay, G., et al. 2003, ApJ, 537, 739
Ginzburg, V.L., & Syrovatskii, S.I. 1964, The Origin of Cosmic Rays, Pergamon Press, New York
Kelner, S.R., Aharonian, F.A., & Vugayov, V.V. 2006, Phys. Rev. D, 74, 034018
Martí, J., Rodríguez, L.F., & Reipurth, B. 1993, ApJ, 416, 208
Martí, J., Rodríguez, L.F., & Reipurth, B. 1995, ApJ, 449, 184
McKee, C.F., & Ostriker, E.C. 2007, ARA&A, 45, 565
Plambeck, R.L., & Menten, K.M. 1990, ApJ, 364, 555
Pravdo, S. H., Tsuboi, Y., & Maeda, Y. 2004, ApJ, 605, 259
Protheroe, R.J. 1999, in: Topics in Cosmic-Ray Astrophysics, 1999, p.247 [astro-ph/9812055]
Rodríguez, L.F., et al. 2005, ApJ 626, 953
Rodríguez, L.F., et al. 2008, AJ 135, 2370
Romero, G. E., Benaglia, P., & Torres, D. F. 1999, A&A, 348, 868
Romero, G. E. 2008, in American Institute of Physics Conference Series, Vol. 1085, eds. F. A. Aharonian, W. Hofmann, & F. Rieger, (Melville:American Institute of Physics Conference Series), p. 97
Shu, F.H, Adams, F.C., & Lizano, S. 1987, ARA&A, 25, 23